ACS APPLIED MATERIALS & INTERFACES

Article

Multifunctional yolk-shell nanostructure as a superquencher for fluorescent analysis of potassium ion using guanine-rich oligonucleotides

Na Lu, Yanli Wen, Gang Liu, Lei Ding, Caixia Zeng, Ali Aldalbahi, Muhammad Khan, Govindasami Periyasami, Mostafizur Rahaman, Abdulaziz Alrohaili, Jiye Shi, Shiping Song, Lihua Wang, and Min Zhang

ACS Appl. Mater. Interfaces, **Just Accepted Manuscript** • DOI: 10.1021/acsami.7b08732 • Publication Date (Web): 17 Aug 2017

ACS Publications

ACS Applied Materials & Interfaces is published by the American Chemical Society.
1155 Sixteenth Street N.W., Washington, DC 20036

Multifunctional yolk-shell nanostructure as a superquencher for fluorescent analysis of potassium ion using guanine-rich oligonucleotides

Na Lu,[†,] Yanli Wen,[‡] Gang Liu,[‡] Lei Ding,[§] Caixia Zeng,[†] Ali Aldalbahi,[#,]* Muhammad Naziruddin Khan,[#] Govindasami Periyasami,[#] Mostafizur Rahaman,[#] Abdulaziz Alrohaili,[#] Jiye Shi,[∥] Shiping Song,[⊥] Lihua Wang,[⊥,]* and Min Zhang[§,]*

[†]School of Materials Engineering, Shanghai University of Engineering Science, Shanghai 201620, China

[‡]Laboratory of Biometrology, Division of Chemistry and Ionizing Radiation Measurement Technology, Shanghai Institute of Measurement and Testing Technology, Shanghai 201203, China

[§]College of Chemistry and Chemical Engineering, Shanghai University of Engineering Science, Shanghai 201620, China

[#]Chemistry Department, King Saud University, Riyadh 11451, Saudi Arabia

[∥]UCB Pharma, 208 Bath Road, Slough, SL1 3WE, UK

[⊥]Division of Physical Biology & Bioimaging Center, Shanghai Synchrotron Radiation Facility, Shanghai Institute of Applied Physics, Chinese Academy of Sciences, Shanghai 201800, China

KEYWORDS: multifunctional yolk-shell nanoparticles, superquencher, fluorescent sensing, potassium ion, G-rich oligonucleotides

ABSTRACT The excellent performance of biosensor generally depends on the high signal-to-noise ratio, and the superquencher plays dominant role on the fluorescent sensors. Novel nanoquenchers exhibited high quenching efficiency in various fluorescent assays of bio/chemical molecules. Here, we developed a novel nanobiosensor using Fe_3O_4@C yolk-shell nanoparticles (YSNPs) and studied their quenching effect. We found the Fe_3O_4@C YSNP was a superquencher and exhibited an ultrastrong quenching ability, up to almost 100% quenching efficiency, toward fluorophores. Also, the Fe_3O_4@C YSNPs possessed the most superior fluorescence restoration efficiency, due to biomolecular recognition event, to the other nanoquenchers, including gold nanoparticles (AuNPs), graphene oxide (GO), and single wall carbon nanotubes (SWCNTs). On the basis of that, a fluorescent sensing platform to potassium ion (K^+) analysis with guanine (G)-rich oligonucleotides was designed. As a result, the Fe_3O_4@C YSNP-based fluorescent sensors demonstrated excellent performance, with an ultrahigh sensitivity of a detection limit as low as 1.3 μM, as well as a wide dynamic range from 50 μM to 10 mM. The proposed method is fast, simple, and cost-effective, suggesting the great potential for practical applications in biomedical detection and clinical diagnosis.

INTRODUCTION

There has been an increasing interest in the development of new tools for fluorescent assaying bio/chemical molecules owing to their intrinsic merits, such as high sensitivity, rapid response, and especially *in vivo* imaging[1,2] properties. A typical design of fluorescent sensor usually consists of a fluorescent dye/quencher pairs to form Förster resonance energy transfer (FRET) through energy transfer and/or electron transfer.[3-5] The fluorescent quenching is closely dependent on the distance between the dye/quencher pairs, which is coupled with structural switching due to biomolecular recognition event, e.g., DNA base pairing and target-aptamer binding. Also importantly, the molecular probes greatly influence the fluorescent quenching efficiency based upon the signal-transduction mechanism, such as the selection and parametric optimization of dye/quencher pairs.

Over the past decades, advances of nanotechnology have brought forth great impacts on biosensing,[6,7] nanomedicine,[8,9] bioimaging,[10,11] and drug delivery.[12,13] Recently, a variety of nanomaterials (NMs) have exhibited remarkably high quenching ability towards a wide spectrum of fluorophores. These nanoquenchers are beneficial for elimination of the selection issue of a dye/quencher pairs thanks to their quenching ability towards different fluorophores with a wide range of emission frequencies, Up till now, zero-dimensional (0D) nanostructures such as gold nanoparticles (AuNPs),[14-16] polydopamine (PDA) nanospheres,[17,18] 1D carbon nanotubes (CNTs),[19-21] and 2D nanosheets such as graphene oxide (GO),[22-24] molybdenum disulfide (MoS_2),[25,26] have been employed as effective nanoquenchers to

construct fluorescent biosensors[27] for nucleic acids, proteins, small molecules and metal ions.[28-30] Nevertheless, the preparation of these materials is also considered to be elaborate, labor-intensive and time-consuming (e.g., GO preparation by Hummers method[31]), and especially some of these materials have nanotoxicity for *in vivo* studies;[32, 33] accordingly, much scientific effort should be directed toward designing and fabricating of new nanoquenchers for fluorescent assays.

Recently, yolk-shell nanoparticles (YSNPs)[34] with movable cores inside hollow shells have drawn a great deal of attention due to their unique and appealing properties such as low density, large specific surface area, and the tailorability and functionality in both the cores and shells. Given these advantages, many efforts have been made to employ in nanoreactors,[35,36] drug delivery,[37,38] lithium-ion batteries,[39] and biocatalysis.[40, 41] Nevertheless, yet to date there has been no report on fluorescence quenching abilities of YSNP, which can be used to develop a novel strategy for FRET-based fluorescent sensor.

In this work, the fluorescent quenching ability of Fe_3O_4@C YSNPs, with Fe_3O_4 cores inside carbon shells, was first studied. Fe_3O_4 cores, as an essential quality, enable easy separation from reacted solution under an external magnetic field without centrifugation or filtration. Due to the large surface area and microporous morphology, the quenching ability of Fe_3O_4@C YSNP was found to be higher than that of other NMs (e.g. bare Fe_3O_4 NPs, SWCNTs). Also, the Fe_3O_4@C YSNPs exhibited the highest fluorescence restoration efficiency among the nanoquenchers. This was then adopted as a sensing platform to potassium ion (K^+) analysis with the assistance of

guanine (G)-rich oligonucleotides based on the fluorescence restoration resulting from binding-induced conformational change. The Fe_3O_4@C YSNP-based fluorescent K^+ sensor exhibited excellent performance with a very high sensitivity and a wide dynamic range, suggesting this proposed method has great potential in practical applications.

MATERIALS AND METHODS

Chemicals and reagents. The carboxyfluorescein(FAM)-labeled oligonucleotides with G-rich human telomere sequence and random sequence were synthesized from Sagnon Biotech. Co. Ltd. (Shanghai, China). The oligonucleotides were purified by HPLC and verified by mass spectra. Tris(hydroxymethyl)aminomethane (≥99.0%) were purchased from Sinopharm Chemical Reagent Co., Ltd (Shanghai, China). Dopamine hydrochloride was obtained from the Alfa Aesar (China) Chemical Co., Ltd. Tetraethoxysilane (TEOS, 95%) was obtained from Energy Chemical Company (Shanghai, China).All chemicals were used without further purification. All solutions were prepared with ultrapure water produced by a Mill-Q Purification System (Millipore, USA).

Instrumentation. Fluorescence spectra were measured on Hitachi F-7000 Fluorescence spectrophotometer (Hitachi High-Technologies Corporation/Hithachi, Ltd., Japan). Absorption spectra for DNA quantification were performed on a Nanodrop 2000 spectrophotometer (Thermo-Fisher Scientific, USA). The concentrations of DNA were determined using the corresponding extinction coefficients. The microstructures of Fe_3O_4@C YSNPs were characterized by

Transmission electron microscopy (TEM, JEOL-1011).

Synthesis of Fe_3O_4@C YSNPs. Fe_3O_4@C YSNPs were prepared by using a one-step facile approach, as reported in the previous work.[42] Firstly, 300 μL of TEOS in the ethanol solution was dropwise added into the mixture of 0.1 g of Fe_3O_4 nanoparticles (NPs) and 2 mL of ammonium hydroxide (NH_4OH). After being stirred for 12 h, 50 mg of dopamine (DA) was introduced and reacted for 24 h under stirring, and thus polydopamine (PDA) layer was formed to obtain Fe_3O_4@SiO_2@PDA NPs. Next, Fe_3O_4@SiO_2@C NPs were obtained by annealing Fe_3O_4@SiO_2@PDA NPs at 500 °C for 4 h. Finally, Fe_3O_4@C YSNPs were prepared through chemical etching of SiO_2 template with ammonium hydroxide in ethanol/water solution.

Optimization. To investigate the effect of ionic strength, 50 nM of the fluorophore (FAM)-labeled single-strand DNA (ssDNA) with random sequence of 5'-FAM-ACCTGGGGGAGTAT-3'(termed as DNA-F*) was firstly heated at 95° C for 5 min and then cooled to room temperature. Then DNA-F* and Fe_3O_4@C YSNPs were mixed containing varied concentration of NaCl (0, 25, 50, and 100 mM) and incubated for 10 min. After removing Fe_3O_4@C YSNPs by external magnetic field, samples were excited with 488 nm laser light, and the emission was measured at 518 nm.

In the time- and concentration-dependent experiments, 50 nM of FAM-labeled DNA with a sequence of 5'-FAM-GGTTGGTGTGGTTGG-3' (termed as G4-F*) was used. In the time-dependent experiments, the incubation time of G4-F*/Fe_3O_4@C YSNPs were 0, 1, 2, 3, 4, 5, 7.5, 10, and 15 min, respectively. In the

concentration-dependent experiments, the final concentrations of Fe_3O_4@C YSNPs were 0, 10, 20, 30, 40, and 50 μg mL^{-1}, respectively. The measuring steps were the same as described above.

In a typical procedure, 50 nM of G4-F*dissolved in Tris-HCl solution (50 mM, pH7.2) was denatured at 95° C for 5 min, followed by quickly cooling to room temperature in an ice water bath to ensure single-stranded form. Subsequently, a Tris-HCl buffer solution containing different concentrations of K^+ ranging from 0 to 10 mM was added into the G4-F* solution, and incubated for 10 min to induce the formation of G-quadruplex. After then, 20 μg mL^{-1} Fe_3O_4@C YSNPs were introduced into the above mixed solution and reacted for 10 min. Finally, the reaction solutions after removing Fe_3O_4@C YSNPs were transferred to a quartz cuvette and recorded with a fluorescence spectrometer.

RESULTS AND DISCUSSION

In this study, we prepared monodisperse Fe_3O_4@C YSNP by a simple and versatile method, according to our previous report.[42] Polydopamine (PDA), as a nontoxic carbon precursor, was prepared through self-polymerization of dopamine (DA) to deposit controlled conformal films on any surface. Fe_3O_4@C YSNP was synthesized by coating double layers of SiO_2 and PDA on Fe_3O_4 core by a one-step method, followed by carbonization and removal of SiO_2 template (Figure 1A). In Figure 1B, scanning electron microscopy (SEM) image clearly reveals that Fe_3O_4@C YSNPs are monodisperse and uniform nanospheres, which has an average diameter of ~200 nm with a void size of ~40 nm. Transmission electron microscopy (TEM) image shows

that Fe_3O_4 cores were encapsulated in hollow carbon shells with a several nanometer thickness full of microporosity (Figue 1C).[43]

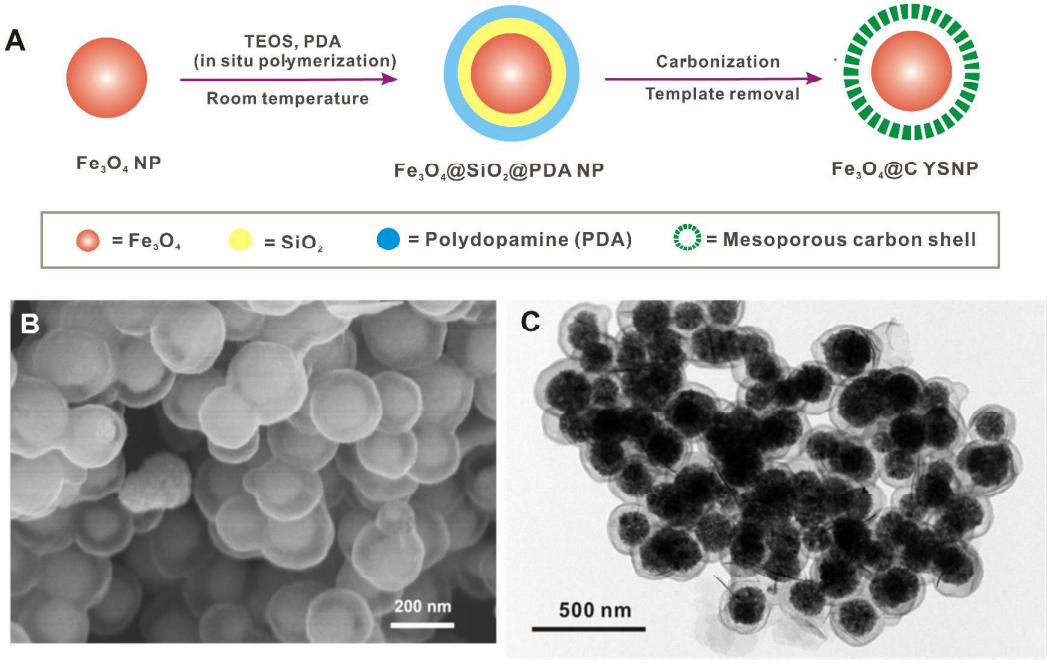

Figure 1. (A) Scheme for the synthesis of Fe_3O_4@C YSNPs. (B, C) Typical SEM (B) and TEM images(C) of as-prepared Fe_3O_4@C YSNPs.

K^+-induced folding of human telomeric DNA into G-quadruplex was utilized as the model system in the proof-of-concept study of the quenching ability of YSNP and fluorescent sensing platform. Figure 2A illustrates the scheme of Fe_3O_4@C YSNP as a quenching probe and fluorescent analysis of K^+ by using G-rich DNA oligonucleotide. A carboxyfluorescein (FAM)-labeled oligonucleotide for K^+ in the single-stranded (ss-) state with soft coil-like structure gave a strong fluorescence in the buffer solution. When Fe_3O_4@C YSNPs were added, ssDNA could bind Fe_3O_4@C YSNPs with high affinity or insert into the micropores on the carbon shells, and the fluorophores were pulled to the surface of YSNP and quenched efficiently, resulting in an effective

quenching of fluorescence. While K^+ induced the structural variation of G-rich sequence into a tertiary structure of four-stranded tetraplex structure with low affinity or inability to being arrested and which produced a strong fluorescence recovery. These formed the foundation of fluorescent sensors for K^+.

To verify the feasibility of the design, an aptamer for K^+ with a sequence of 5'-FAM-GGTTGGTGTGGTTGG-3' (termed as G4-F* in the following text) was used in the experiments. The quenching efficiency (QE) of Fe_3O_4@C YSNP for G4-F*and FR after target-binding were first studied. Here, QE was calculated according to the formula: QE = $(1-F_0/F_b) \times 100\%$, where F_0 and F_b are fluorescence intensities in the presence and absence of Fe_3O_4@C YSNPs, respectively. Initially, 50 nM of G4-F* ssDNA displayed a strong fluorescence in Tris-HCl buffer solution (pH 7.2) (curve a in Figure 2B). Upon addition of 20 μg mL^{-1} of Fe_3O_4@C YSNPs, there was a conspicuous decline in G4-F* fluorescence after collecting the magnetic Fe_3O_4@C YSNPs under an external magnetic field with the help of magnetic properties of Fe_3O_4 cores (curve b in Figure 2B).The QE continuously increased with the amount of Fe_3O_4@C YSNPs, which was almost totally quenched in the concentration of 50 μg mL^{-1} (Figure 3C). For bare Fe_3O_4 NPs, the QE for FAM-ssDNA was reported to be ~75%.[44] In contrast, Fe_3O_4@C YSNPs exhibited higher fluorescence QE than that of other NMs, such as bare Fe_3O_4 NPs, GO, and SWCNTs in the same ratios of fluorescent DNA to NM probes.[45]

Also, fluorescence restoration (FR) of the Fe_3O_4@C YSNP plays vitally important role in the fluorescent sensors. Curve c in Figure 2B shows a noteworthy

enhancement in fluorescence intensity (FI) in the presence of K^+. We defined the FR = $(F\text{-}F_0)/(F_b\text{-}F_0)\times100\%$, where F_b is the initial value before adding Fe_3O_4@C YSNPs, F_0 is the intensity in the absence of K^+, and F is the intensity in the presence of K^+. The FR for different samples were presented is Figure 2C. The FR for blank sample containing only G4-F* was set as 100%. When Fe_3O_4@C YSNPs were introduced, the fluorescence was quenched with maximum efficiency and the FR for G4-F*/Fe_3O_4@C YSNP was zero. In the presence of K^+ (10 mM), the FR for G4-F*/Fe_3O_4@C YSNP/K^+ was calculated to be as high as 62%, while that of AuNPs, GO, and SWCNTs was only 3.1%, 34%, and 29%, respectively (Table S2).[45] It is clearly shown that the YSNP has the highest restoration efficiency among the nanoquenchers, implying their potential use in YSNP-based sensors.

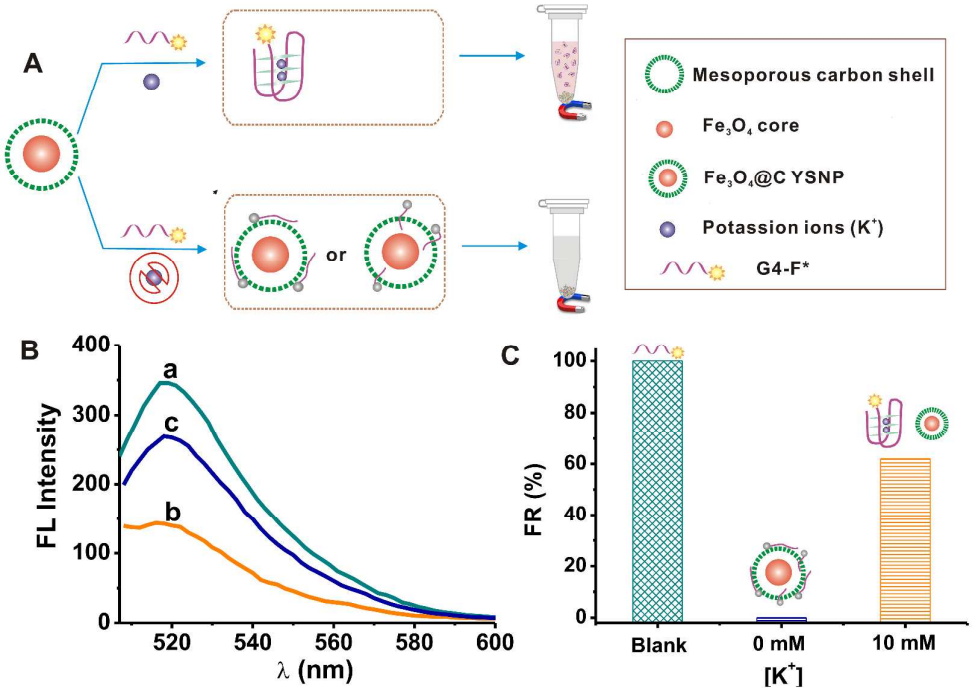

Figure 2. (A) Schematic illustration of Fe_3O_4@C YSNP as an efficient nanoquencher

and fluorescent analysis of K^+ using G-rich oligonucleotides. (B) Fluorescence spectra of G4-F* (a), G4-F*/Fe_3O_4@C YSNPs (b), and K^++G4-F*/ Fe_3O_4@C YSNPs (c). (C) The fluorescence restoration (FR) for G4-F* (blank), G4-F*/Fe_3O_4@C YSNP (0 mM K^+), and G4-F*/Fe_3O_4@C YSNP/K^+ (10 mM K^+). The concentrations of G4-F*, Fe_3O_4@C YSNs, and K^+ are 50 nM, 20 μg mL^{-1}, and 10 mM, respectively.

It is well known that ionic strength plays an important role that can modulate electrostatic interactions in many biosensors. Especially for nanoparticle-based biosensor, a high ionic strength is prerequisite to stabilize nanoparticle suspensions to prevent them from aggregation.[46-48] Besides, the detecting sensitivity of field effect transistor (FET) device in a high salt solution is fundamentally hindered by Debye screening.[49,50] To study the influence of ionic strength, we used a FAM-labeled DNA with random sequence of 5'-FAM-ACCTGGGGGAGTAT-3' (termed as DNA-F* in the following text) which cannot fold into G-quadruplex in high salt solution. As shown in Figure 3A, fluorescence spectra of DNA-F*/Fe_3O_4@C YSNPs were measured in Tris-HCl buffer solutions containing varied concentrations of salt (NaCl). Interestingly, it must be noted that a dramatic fluorescence decrease still produced even in a no/low NaCl solution after incubation with Fe_3O_4@C YSNPs, which almost equaled to the changes of that with high salt. It suggested that efficient quenching can take place in solutions with no/low NaCl.

In addition, we investigated the effects of several other experimental conditions, such as incubation time of G4-F*/Fe_3O_4@C YSNPs, and the concentration of

Fe_3O_4@C YSNPs. Figure 3B shows the influence of time on the fluorescence response of G4-F*/Fe_3O_4@C YSNPs. The fluorescence intensity continuously decreased along with the time. After 10 min, ~80% of initial fluorescence intensity was quenched and it remained nearly constant. Hence, we selected 10 min as the optimized incubation time for fluorescence assays. The concentration of Fe_3O_4@C YSNPs also significantly affected the fluorescence of G4-F*. It was observed that there was gradual reduction in the fluorescence response with the increasing amount of Fe_3O_4@C YSNPs (Figure 3C). The fluorescence response plotted as a linear function of the concentration of Fe_3O_4@C YSNPs (Figure 3D), which was totally quenched at the concentration of 50 μg mL^{-1}, suggesting that multifunctional Fe_3O_4@C YSNPs can be employed as an excellent probe in fluorescence assays.

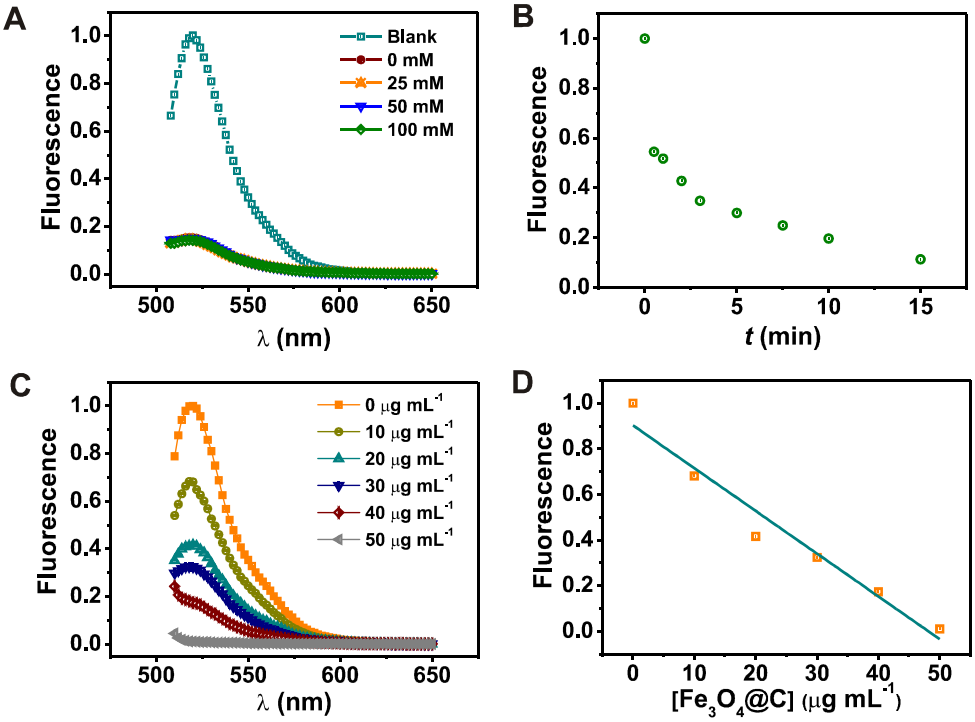

Figure 3. (A) Fluorescence spectra of DNA-F*/Fe_3O_4@C YSNPs with varied

concentration of NaCl. (B) Time-dependent fluorescence responses of G4-F*/Fe_3O_4@C YSNPs. (C) Fluorescence spectra of G4-F* with different concentration of Fe_3O_4@C YSNPs. (D) The relationship between fluorescence intensity of G4-F* and the concentration of Fe_3O_4@C YSNPs.

To obtain a high sensitivity and a wide dynamic range, we also explored the optimal concentration of Fe_3O_4@C YSNPs on fluorescent K^+ sensor. Experiments were carried out at a fixed concentration of 50 nM G4-F* with varied concentration of K^+, incubating with different amount of Fe_3O_4@C YSNPs, respectively. When 25 μg mL^{-1} of Fe_3O_4@C YSN was added, K^+ at the concentration of 1 mM, 10 mM, and 30 mM exhibited different fluorescence enhancement and the FR were 16%, 20%, and 40%, respectively (Figure 4A). Whereas, almost no obvious fluorescence enhancement was found with 50 μg $mL^{-1}$of Fe_3O_4@C YSNs, even if the concentration of K^+ was as high as 100 mM (Figure 4B). The reason might be that a higher concentration of YSNPs could interact with more DNA molecules on their surface and leave very few DNA molecules free the aqueous solution. When K^+ is introduced at the concentration of 1 mM and 10 mM, it shows that the FR respectively reached approximate 40% and 62% with 20 μg mL^{-1} of Fe_3O_4@C YSNPs, which has a much larger fluorescence change than that at the amount of 25 μg mL^{-1} and 50 μg mL^{-1} (Figure 4C). Hence, 20 μg mL^{-1} of Fe_3O_4@C YSNPs was selected as the optimal concentration in the fluorescent sensing of K^+.

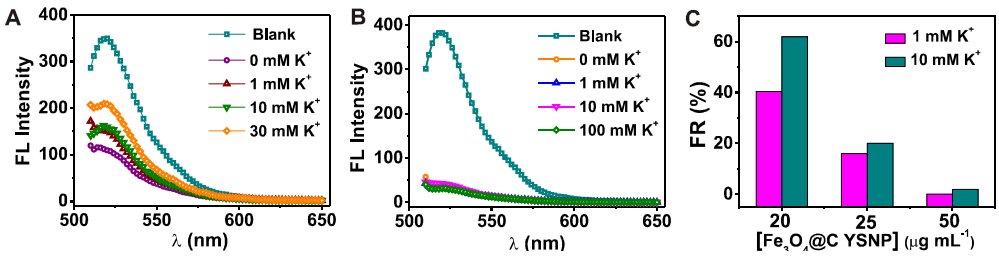

Figure 4. (A, B) Fluorescence spectra of 50 nM G4-F* incubated with 25 μg mL^{-1} (A) and 50 μg mL^{-1} (B) of Fe_3O_4@C YSNPs in the presence of different amounts of K^+. Blank represents the sample without Fe_3O_4@C YSNPs and K^+. (C) Comparison of FR in the presence of 1 mM and 10 mM of K^+ under different concentrations of Fe_3O_4@C YSNPs.

To investigate the feasibility of the fluorescent sensor based upon Fe_3O_4@C YSNP as a superquencher and DNA aptamer, we have explored the quantitative analysis of this sensor toward K^+ under the optimal conditions. As shown in Figure 5A, typical fluorescence spectra corresponding to a series of concentrations of K^+ (0 mM, 0.05 mM, 0.1 mM, 0.5 mM, 5 mM, and 10 mM) has been tested in assay solutions. With the addition of the target, fluorescence response is gradually going up with the increase of K^+ concentration. It shows a FR of almost 30% when the concentration of K^+ is as low as 50 μM (Figure S1). As can be seen from Figure 5B, the calibration plot showed there was a good linear relationship between fluorescence intensity and the logarithm of K^+ concentration. The dynamic range is suitable for the physiological potassium level (3.50-5.30 mM). A limit of detection (LOD) as low as 1.3 μM could be obtained according to the assumption of a signal greater than that of three times of the measurement standard error (3σ) of a non-target blank sample. As illustrated in

Table S1, our sensor has very excellent performance with a much higher sensitivity and a wider dynamic range comparing with that of other reported K^+ sensing platform. Besides that, our method has several additional advantages of cost-effectiveness, easier to operation, and rapid detection, indicating that it is applicable to detect K^+ in various fields. To further examine the selectivity of the Fe_3O_4@C YSNP-based fluorescent sensor, some other different anions were chosen as potentially interfering substances and their fluorescent responses have been investigated. As shown in Figure 5C, 10 mM K^+ induced a strong fluorescence intensity, whereas the presence of other interfering anions produced little signal responses even if their concentrations (50 mM) were 5 times higher than that of K^+. This excellent selectivity may be attributed to the high specificity between G-rich aptamer and its target (K^+), as well as interfering anions with larger charger intensity resulting in much higher binding affinities between ssDNA and Fe_3O_4@C YSNP so that the fluorescence can not be recovered.

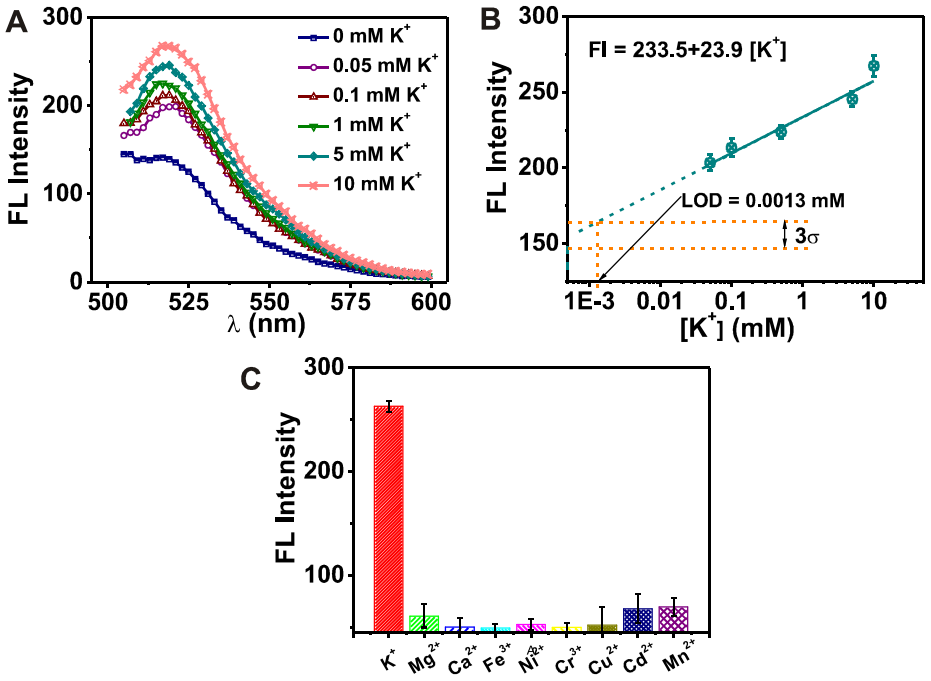

Figure 5. Fluorescence spectra (A) and calibration curve (B) for K^+ detection using 20 μg mL^{-1} of Fe_3O_4@C YSNPs as nanoquenchers and 50 nM G-rich oligonucleotides. (C) The fluorescence intensity of Fe_3O_4@C YSNP/G4-F* complex in the presence of K^+ (10 mM) and other interfering anions (50 mM). The error bars represent the standard deviation of three measurements.

As described above, Fe_3O_4@C YSNP demonstrated superquenching abilities and the highest FR efficiency with ssDNA molecules. Consequently, the Fe_3O_4@C YSNP-based fluorescent sensors exhibited a greatly enhanced sensitivity and a wide dynamic range required in biomedical research and practical diagnosis. In view of their structural features and component, we believe that the excellent performance of the fluorescent sensors is highly related with the physical and chemical properties of Fe_3O_4@C YSNPs as well as their distinctive nanostructures. What's more, the occupied space of ssDNA on the Fe_3O_4@C YSNP surface was analyzed and compared with other NMs. The surface area of Fe_3O_4@C YSNPs, the surface density and the surface coverage of ssDNA were listed in Table S2. Under optimal conditions (20 μg mL^{-1}), Fe_3O_4@C YSNPs had a surface area of 80.4 cm^2, and the ssDNA surface density and the surface coverage were $7.5\times10^{10}/cm^2$ and 0.13%, respectively. Notably, Fe_3O_4@C YSNPs possess the lowest surface density and surface coverage among the listed NMs, implying that all DNA molecules have more space to occupy or anchor on the surface and thus result in an ultrahigh quenching. The ultralow surface coverage may attribute to the porous carbon shell with extremely large surface

area (2006 m^2 g^{-1}).[51] Moreover, the Fe_3O_4 cores are encapsulated protected by the outer carbon shell protected from aggregation and poisoning. Multifunctional Fe_3O_4@C YSNPs possess excellent magnetic properties, in which nanomaterials quickly separated to the side of the vial within seconds. The magnetic nature can be applied for effective separation and concentration in complicated matrices, such as in living systems.

Additionally, we deemed that the fluorescence quenching of Fe_3O_4@C YSNPs for ssDNA may be realized through two ways (Figure 6). Electroactive pyridinic N and graphitic N has been reported to be detectable in PDA-based carbon shells.[50] DNA strands are composed of monomer units, consisting of positively charged nitrogenous bases and negatively charged phosphate backbone. One way is that the binding between Fe_3O_4@C YSNP and ssDNA is likely to be occurred through non-covalent interactions, including π-π stacking, hydrogen bonding, or energy/electron transfer between the unit of nucleotide and YSNP. Moreover, Fe_3O_4@C YSNPs possessed the morphology with both micropores (≤ 2 nm) and mesopores (2~50 nm) on the surface of the carbon shells, in which micropores were in the majority.[50] Therefore, the other quenching way is, due to size effect, ssDNA (1.5 nm) was arrested by micropore and thus led to a high-efficiency fluorescence quenching even in low salt solution, which is consistent with the forgoing phenomena. Nevertheless, the detailed mechanism has not been fully understood still.

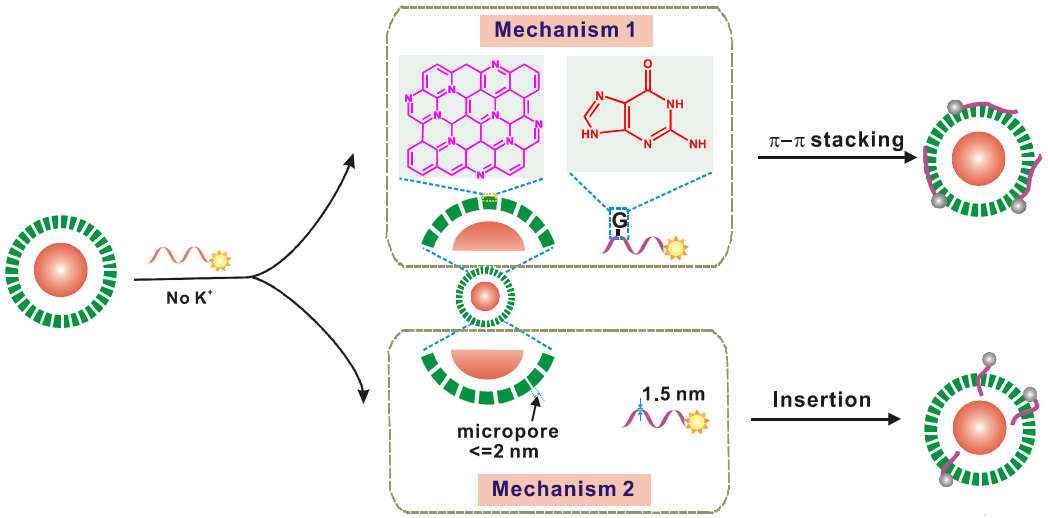

Figure 6. Two quenching ways of Fe_3O_4@C YSNP for ssDNA.

Previous literature has reported that sodium ions (Na^+) also can drive the folding of oligonucleotide models of human telomere DNA into G-quadruplex structures.[52] Therefore, an "OR" logic gate system was constructed by utilizing K^+ or Na^+ as inputs that were based on a combination of Fe_3O_4@C YSNPs and G-quadruplex DNA sequences. Figure 7A outlines the schematic illustration to construct the "OR" gate. We used either K^+ or Na^+ as inputs to activate the self-assembly of G-quadruplex, which yielded the fluorescence of G4-F* as output and readout signal. That is, the fluorescence is excited when any of the ions inputs was present in the system, K^+ or Na^+, (1, 0), (0, 1) or the coexistence of both the two ion-inputs (1, 1), as shown in the truth table (Figure 7B). Figure 7C displays the experimental results upon activating by the input-ion. The fluorescence has a low intensity in the absence of any ion-input (0, 0) (curve a, Figure 7C), while the system is subjected to either K^+ or Na^+ yields high intensity of fluorescence (curve b, c, Figure 7C). Also, as the system is activated by both inputs, a "true" output is observed in curve d. The relative fluorescence change

(defined as $(F-F_0)/F_0$) of the "OR" gate system in the form of bars are illustrated in Figure 7D.

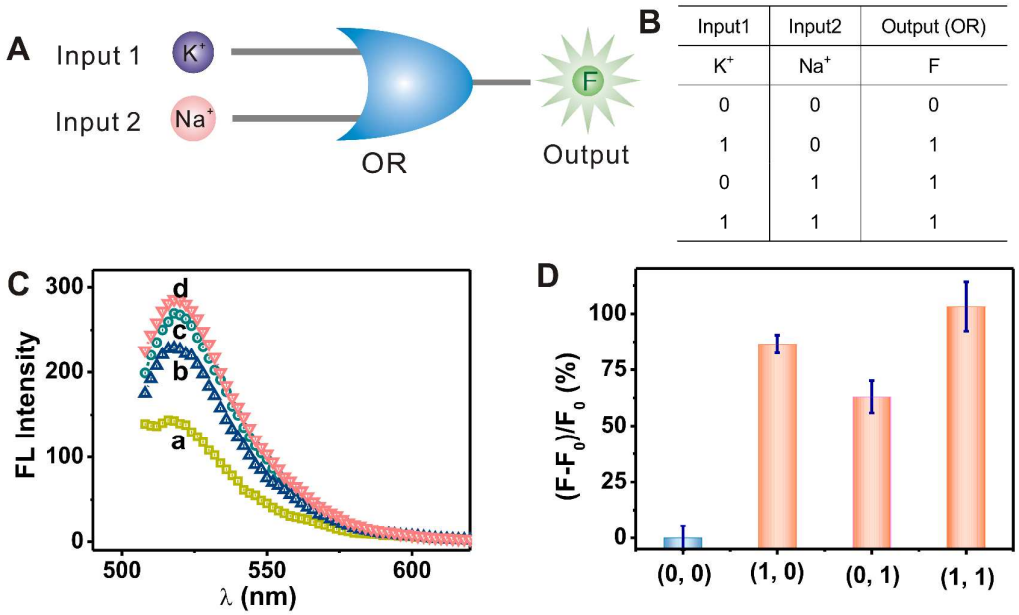

Figure 7. (A) An "OR" logic gate system consisting of Fe_3O_4@C YSNPs and guanine-rich aptamer that are activated by K^+ or Na^+ as inputs. (B) Truth table of the "OR" logic gate system. (C) Fluorescence spectra of the "OR" logic gate system activated by the following inputs: (a) no K^+, no Na^+, (b) K^+, (c) Na^+, and (d) K^++Na^+. (D) The relative fluorescence change in the form of bars presentation. The error bars represent the standard deviation of three measurements.

CONCLUSION

In summary, it has been demonstrated for the first time that Fe_3O_4@C YSNPs showed superstrong quenching abilities and ultrahigh FR efficiency towards FAM-labelled ssDNA. It was found that the quenching efficiency was up to almost 100%. Additionally, Fe_3O_4@C YSNPs possessed a much higher FR efficiency in the presence of K^+ than other nanoquenchers, such as AuNPs, GO, and SWCNTs. Based

on these findings, Fe_3O_4@C YSNPs were used as a fluorescent sensor toward K^+ with G-rich oligonucleotides, exhibiting excellent performance of a much higher sensitivity and a wider dynamic range. Moreover, an "OR" logic gate system with multiplex detection capability for K^+ and Na^+ was built. The proposed method is fast, easy to operate, low-cost, and easy separation under an external magnetic field without centrifugation or filtration. In view of these advantages, this sensing platform could offer a promising tool for practical applications in molecular diagnosis and point-of-care test (POCT).

ASSOCIATED CONTENT

Supporting Information

Fluorescence restoration with varied concentrations of K^+ under the optimal conditions. Comparison with other reported K^+ sensing platforms. The properties of NM-based fluorescent sensors. This material is available free of charge via the Internet at http://pubs.acs.org.

AUTHOR INFORMATION

Corresponding Author

*E-mail addresses: aaldalbahi@ksu.edu.sa, (A. Aldalbahi), wanglihua@sinap.ac.cn (L. Wang), zhangmin@sues.edu.cn (M. Zhang).

ACKNOWLEDGMENTS

This work was financially supported by National Key Research and Development Program (2016YFA0201204, 2013CB933802), Shanghai Municipal Natural Science Foundation (17ZR1412100), Key Laboratory of Interfacial Physics and Technology, Chinese Academy of Sciences (CASKL-IPT1603), Startup Foundation for Doctors of Shanghai University of Engineering Science, the National Natural Science Fund of China (21373260, 31470960). Ali Aldalbahi acknowledges the financial support by Deanship of Scientific Research, College of Science Research Center, King Saud University.

REFERENCES

(1) Smith, B. R.; Gambhir, S. S. Nanomaterials for In Vivo Imaging. *Chem. Rev.* **2017,** *117*, 901-986.

(2) Dubertret, B.; Skourides, P.; Norris, D. J.; Noireaux, V.; Brivanlou, A. H.; Libchaber, A. In Vivo Imaging of Quantum Dots Encapsulated in Phospholipid Micelles. *Science* **2002,** *298*, 1759-1762.

(3) Pei, H.; Liang, L.; Yao, G.; Li, J.; Huang, Q.; Fan, C. Reconfigurable Three-Dimensional DNA Nanostructures for the Construction of Intracellular Logic Sensors. *Angew. Chem. Int. Edit.* **2012,** *51*, 9020-9024.

(4) Nagatoishi, S.; Nojima, T.; Juskowiak, B.; Takenaka, S. A Pyrene-labeled G-quadruplex Oligonucleotide as a Fluorescent Probe for Potassium Ion Detection in Biological Applications. *Angew. Chem. Int. Edit.* **2005,** *44*, 5067-5070.

(5) Ueyama, H.; Takagi, M.; Takenaka, S. A Novel Potassium Sensing in Aqueous

Media with a Synthetic Oligonucleotide Derivative. Fluorescence Resonance Energy Transfer Associated with Guanine Quartet-Potassium Ion Complex Formation. *J. Am. Chem. Soc.* **2002,** *124*, 14286-14287.

(6) Zhu, C.; Yang, G.; Li, H.; Du, D.; Lin, Y.; Chem, A. Electrochemical Sensors and Biosensors Based on Nanomaterials and Nanostructures. *Anal. Chem.* **2015,** *87*, 230-249.

(7) Ge, Z. L.; Hao, P.; Wang, L. H.; Song, S. P.; Fan, C. H. Electrochemical Single Nucleotide Polymorphisms Genotyping on Surface Immobilized Three-Dimensional Branched DNA Nanostructure. *Sci. China Chem.* **2011,** *54*, 1273-1276.

(8) Riehemann, K.; Schneider, S. W.; Luger, T. A.; Godin, B.; Ferrari, M.; Fuchs, H. Nanomedicine--Challenge and Perspectives. *Angew. Chem. Int. Edit.* **2009,** *48*, 872-897.

(9) Chen, G.; Roy, I.; Yang, C.; Prasad, P. N. Nanochemistry and Nanomedicine for Nanoparticle-based Diagnostics and Therapy. *Chem. Rev.* **2016,** *116*, 2826-2885.

(10) Wolfbeis, O. S. An Overview of Nanoparticles Commonly Used in Fluorescent Bioimaging. *Chem. Soc. Rev.* **2015,** *44*, 4743-4768.

(11) Yuan, L.; Lin, W.; Zheng, K.; Zhu, S. FRET-Based Small-molecule Fluorescent Probes: Rational Design and Bioimaging Applications. *Accounts Chem. Res.* **2016,** *46*, 1462-1473.

(12) Farokhzad, O. C.; Langer, R. Impact of Nanotechnology on Drug Delivery. *ACS Nano* **2009,** *3*, 16-20.

(13) Li, H.; Liu, C.; Zeng, Y. P.; Hao, Y. H.; Huang, J. W.; Yang, Z. Y.; Li, R.

Nanoceria-Mediated Drug Delivery for Targeted Photodynamic Therapy on Drug-Resistant Breast Cancer. *ACS Appl. Mater. Interfaces* **2016,** *8*, 31510-31523.

(14) Lee, J. S.; Han, M. S.; Mirkin, C. A. Colorimetric Detection of Mercuric ion (Hg^{2+}) in Aqueous Media Using DNA-Functionalized Gold Nanoparticles. *Angew. Chem. Int. Edit.* **2007,** *119*, 4171-4174.

(15) Reinhard, B. M.; Siu, M.; Agarwal, H.; Alivisatos, A. P.; Liphardt, J. Calibration of Dynamic Molecular Rulers Based on Plasmon Coupling Between Gold Nanoparticles. *Nano Lett.* **2005,** *5*, 2246-2252.

(16) Chen, P.; Pan, D.; Fan, C.; Chen, J.; Huang, K.; Wang, D.; Zhang, H.; Li, Y.; Feng, G.; Liang, P. Gold Nanoparticles for High-throughput Genotyping of Long-range Haplotypes. *Nat. Nanotechnol.* **2011,** *6*, 639-644.

(17) Qiang, W.; Li, W.; Li, X.; Chen, X.; Xu, D. Bioinspired Polydopamine Nanospheres: a Superquencher for Fluorescence Sensing of Biomolecules. *Chem. Sci.* **2014,** *5*, 3018-3024.

(18) Fan, D.; Wang, E.; Dong, S. Exploiting Polydopamine Nanospheres to DNA Computing: A Simple, Enzyme-Free and G-Quadruplex-Free DNA Parity Generator/Checker for Error Detection during Data Transmission. *ACS Appl. Mater. Interfaces* **2017,** *9*, 1322-1330.

(19) Baughman, R. H.; Zakhidov, A. A.; Heer, W. A. D. Carbon Nanotubes. *Science* **2002,** *297*, 787-793.

(20) Tans, S. J.; Verschueren, A. R. M.; Dekker, C. Room-Temperature Transistor Based on A Single Carbon Nanotube. *Nature* **1998,** *393*, 49-52.

(21) Agrawal, R.; Nieto, A.; Chen, H.; Mora, M.; Agarwal, A. Nanoscale Damping Characteristics of Boron Nitride Nanotubes and Carbon Nanotubes Reinforced Polymer Composites. *ACS Appl. Mater. Interfaces* **2013,** *5*, 12052-12057.

(22) Marcano, D. C.; Kosynkin, D. V.; Berlin, J. M.; Sinitskii, A.; Sun, Z.; Slesarev, A.; Alemany, L. B.; Lu, W.; Tour, J. M. Improved Synthesis of Graphene Oxide. *ACS Nano* **2010,** *4*, 4806-4814.

(23) Geim, A. K. Graphene: Status and Prospects. *Science* **2009,** *324*, 1530-1534.

(24) Manapat, J. Z.; Mangadlao, J. D.; Tiu, B. D.; Tritchler, G. C.; Advincula, R. C. High-Strength Stereolithographic 3D Printed Nanocomposites: Graphene Oxide Metastability. *ACS Appl. Mater. Interfaces* **2017,** *9*, 10085-10093.

(25) Yin, Z.; Li, H.; Li, H.; Jiang, L.; Shi, Y.; Sun, Y.; Lu, G.; Zhang, Q.; Chen, X.; Zhang, H. Single-Layer MoS_2 Phototransistors. *ACS Nano* **2017,** *6*, 74-80.

(26) Mak, K. F.; He, K.; Lee, C.; Lee, G. H.; Hone, J.; Heinz, T. F.; Jie, S. Tightly Bound Trions in Monolayer MoS_2. *Nature Materials* **2013,** *12*, 207-211.

(27) Li, D.; Song, S.; Fan, C. Target-Responsive Structural Switching for Nucleic Acid-Based Sensors. *Accounts Chem. Res.* **2010,** *43*, 631-641.

(28) Lu, C.; Yang, H.; Zhu, C.; Chen, X.; Chen, G. A Graphene Platform for Sensing Biomolecules. *Angew. Chem.* **2009,** *48*, 4785-4787.

(29) Huang, D.; Niu, C.; Wang, X.; Lv, X.; Zeng, G. "Turn-on" Fluorescent Sensor for Hg^{2+} Based on Single-Stranded DNA Functionalized Mn: CdS/ZnS Quantum Dots and Gold Nanoparticles by Time-Gated Mode. *Anal. Chem.* **2013,** *85*, 1164-1170.

(30) Zhu, C.; Zeng, Z.; Li, H.; Li, F.; Fan, C.; Zhang, H. Single-Layer MoS_2-Based

Nanoprobes for Homogeneous Detection of Biomolecules. *J. Am. Chem. Soc.* **2013,** *135*, 5998-6001.

(31) Hummers, W. S.; Offeman, R. E. Preparation of Graphitic Oxide. *J. Am. Chem. Soc.* **1958,** *80*, 1339-1339.

(32) Eldakdouki, M. H.; Xia, J.; Zhu, D. C.; Kavunja, H.; Grieshaber, J.; O'Reilly, S.; McCormick, J. J.; Huang, X. Assessing the In Vivo Efficacy of Doxorubicin Loaded Hyaluronan Nanoparticles. *ACS Appl. Mater. Interfaces* **2014,** *6*, 697-705.

(33) Fischer, H. C.; Chan, W. C. Nanotoxicity: the Growing Need for In Vivo Study. *Curr. Opin. Biotech.* **2007,** *18*, 565-571.

(34) Liu, J.; Qiao, S. Z.; Budi, H. S.; Lu, G. Q. Monodisperse Yolk-Shell Nanoparticles with A Hierarchical Porous Structure for Delivery Vehicles and Nanoreactors. *Angew. Chem. Int. Edit.* **2010,** *49*, 4981-4985.

(35) Kamata, K.; Lu, Y.; Xia, Y. Synthesis and Characterization of Monodispersed Core-Shell Spherical Colloids with Movable Cores. *J. Am. Chem. Soc.* **2003,** *125*, 2384-2385.

(36) Ding, S.; Chen, J. S.; Qi, G.; Duan, X.; Wang, Z.; Giannelis, E. P.; Archer, L. A.; Lou, X. W. Formation of SnO_2 Hollow Nanospheres inside Mesoporous Silica Nanoreactors. *J. Am. Chem. Soc.* **2011,** *133*, 21-23.

(37) Li, Y.; Li, N.; Pan, W.; Yu, Z.; Yang, L.; Tang, B. Hollow Mesoporous Silica Nanoparticles with Tunable Structures for Controlled Drug Delivery. *ACS Appl. Mater. Interfaces* **2017**, *9*, 2123-2129.

(38) Zhao, W.; Chen, H.; Li, Y.; Li, L.; Lang, M.; Shi, J. Uniform Rattle-type Hollow

Magnetic Mesoporous Spheres as Drug Delivery Carriers and their Sustained-Release Property. *Adv. Funct. Mater.* **2008,** *18*, 2780-2788.

(39) Liu, J.; Qiao, S. Z.; Chen, J. S.; Lou, X. W.; Xing, X.; Lu, G. Q. Yolk/shell Nanoparticles: New Platforms for Nanoreactors, Drug Delivery and Lithium-Ion Batteries. *Chem. Commun.* **2011,** *47*, 12578-12591.

(40) Zhou, L.; Kuai, L.; Li, W.; Geng, B. Ion-Exchange Route to Au-Cu_XO_S Yolk-Shell Nanostructures with Porous Shells and Their Ultrasensitive H_2O_2 detection. *ACS Appl. Mater. Interfaces* **2012,** *4*, 6463-6467.

(41) Guo, A.; Li, Y.; Wei, C.; Meng, X.; Dan, W.; Qin, W.; Du, B. An Electrochemical Immunosensor for Ultrasensitive Detection of Carbohydrate Antigen 199 Based on Au@$CuxO_S$ Yolk-Shell Nanostructures with Porous Shells as Labels. *Biosens. Bioelectron.* **2014,** *63*, 39-46.

(42) Lu, N.; Zhang, M.; Ding, L.; Zheng, J.; Zeng, C.; Wen, Y.; Liu, G.; Aldalbahi, A.; Shi, J.; Song, S.; Zuo, X.; Wang, L. Yolk-Shell Nanostructured Fe_3O_4@C Magnetic Nanoparticles with Enhanced Peroxidase-Like Activity for Label-Free Colorimetric Detection of H_2O_2 and Glucose. *Nanoscale* **2017,** *9*, 4508-4515.

(43) Liu, R.; Mahurin, S. M.; Li, C.; Unocic, R. R.; Idrobo, J. C.; Gao, H.; Pennycook, S. J.; Dai, S. Dopamine as A Carbon Source: the Controlled Synthesis of Hollow Carbon Spheres and Yolk-Structured Carbon Nanocomposites. *Angew. Chem.* **2011,** *50*, 6799-6802.

(44) Tong, L. L.; Chen, Z. Z.; Jiang, Z. Y.; Sun, M. M.; Li, L.; Liu, J.; Tang, B. Fluorescent Sensing of Pyrophosphate Anion in Synovial Fluid Based on

DNA-attached Magnetic Nanoparticles. *Biosens. Bioelectron.* **2015,** *72*, 51-55.

(45) Li, F.; Pei, H.; Wang, L.; Lu, J.; Gao, J.; Jiang, B.; Zhao, X.; Fan, C. Nanomaterial-Based Fluorescent DNA Analysis: A Comparative Study of the Quenching Effects of Graphene Oxide, Carbon Nanotubes, and Gold Nanoparticles. *Adv. Funct. Mater.* **2013,** *23*, 4140-4148.

(46) Xia, F.; Zuo, X.; Yang, R.; Xiao, Y.; Kang, D.; Vallée-Bélisleb, A.; Gong, X.; Yuen, J. D.; Hsu, B. B.; Heeger, A. J. Colorimetric Detection of DNA, Small Molecules, Proteins, and Ions Using Unmodified Gold Nanoparticles and Conjugated Polyelectrolytes. *P. Natl. Acad. Sci. USA* **2010,** *107*, 10837-10841.

(47) Yao, G.; Li, J.; Chao, J.; Pei, H.; Liu, H.; Zhao, Y.; Shi, J.; Huang, Q.; Wang, L.; Huang, W. Gold-Nanoparticle-Mediated Jigsaw-Puzzle-like Assembly of Supersized Plasmonic DNA Origami. *Angew. Chem. Int. Ed.* **2015,** *54*, 2966-2969.

(48) Li, H.; Rothberg, L. Colorimetric Detection of DNA Sequences Based on Electrostatic Interactions with Unmodified Gold Nanoparticles. *P. Natl. Acad. Sci. USA* **2004,** *101*, 14036-14039.

(49) Eric Stern, R. W. F. J. S. R. B. T. M. F. M. A. R. Importance of the Debye Screening Length on Nanowire Field Effect Transistor Sensors. *Nano Lett.* **2007,** *7*, 3405-3409.

(50) Lu, N.; Dai, P.; Gao, A.; Valiaho, J.; Kallio, P.; Wang, Y.; Li, T. Label-Free and Rapid Electrical Detection of hTSH with CMOS-Compatible Silicon Nanowire Transistor Arrays. *ACS Appl. Mater. Interfaces* **2014,** *6*, 20378-20384.

(51) Ai, K.; Liu, Y.; Ruan, C.; Lu, L.; Lu, G. M. Sp2 C-dominant N-Doped Carbon

Sub-micrometer Spheres with A Tunable Size: A Versatile Platform for Highly Efficient Oxygen-Reduction Catalysts. *Adv. Mater.* **2012,** *25*, 998-1003.

(52) Gray, R. D.; Chaires, J. B. Kinetics and Mechanism of K^+- and Na^+-Induced Folding of Models of Human Relomeric DNA into G-quadruplex Structures. *Nucleic Acids Res.* **2008,** *36*, 4191-4203.

Table of Contents (TOC)